


An Over-Segmentation-Based Uphill Clustering Method for Individual Trees Extraction in Urban Street Areas From MLS Data

Jintao Li , Xiaojun Cheng, Zhenlun Wu, and Wang Guo

Abstract—In this article, an over-segmentation-based uphill clustering method for individual extraction of urban street trees from mobile laser scanning data is proposed to solve the problem that the existing methods depend heavily on tree trunks and have poor extraction results in complex environments where the tree trunks are blocked by cars and green belts, and the crown touching or interlocking is large. First, supervoxels are generated by over-segmentation, so that the amount of original data is reduced and the boundaries of different objects are effectively preserved. Then, the potential tree crowns and trunks are obtained by extracting typical object structures. Finally, individual trees extraction is realized by extracting independent crowns from the potential crowns via uphill clustering and searching corresponding trunks from the potential trunks. The main contribution of this article is to propose an individual extraction method for street trees based on uphill clustering that does not rely on the extraction of tree trunks, which improves the completeness of extracted results in complex urban environments. The experimental results demonstrate that the proposed method effectively extracted the street trees individually from the test data, with the completeness of 100%, the correctness of 96.4%, and the F -score of 0.98. Moreover, the proposed method also achieves good result for the extraction of greening trees that are heavily blocked in the green belt areas. And the corresponding completeness, correctness, and the F -score are 94.6%, 83.3%, and 0.89, respectively.

Index Terms—Clustering, individual tree, mobile laser scanning (MLS), segmentation, supervoxel, urban environment.

I. INTRODUCTION

As an important part of city, street trees play a crucial role in many aspects like reducing noise [1], improving air quality [2], and increasing urban vegetation coverage [3]. In some other

aspects, it is very important to accurately extract individual street trees and further capture their attributes such as the position, tree height, crown area, and diameter at breast height [4]. For example, the proper planning based on the determination for the number and size of the street trees can minimize losses during road widening [5]. In addition, analyzing the visibility of traffic signs and traffic lights with the individual trees can guarantee the safety of driving. Besides, in power lines inspection aspect, calculating the distances between tree crowns and power lines can discover the potential safety hazards timely and ensure the safety operation of power lines. Moreover, extracting each street tree accurately is also one of the important contents for high-precision structured mapping in urban areas. Therefore, it is of great significance to accurately extract individual trees in urban street areas.

The mobile laser scanning (MLS) technology can quickly obtain the surface information of urban street objects, which are represented by the highly dense point cloud data [6]. Compared with the terrestrial laser scanning, airborne laser scanning (ALS), and digital satellite imaging technologies, MLS technology is more flexible and efficient [7]. In the past, most state-of-the-art surveys for static objects in urban areas were mainly related to the data derived from images. With the rapid development of MLS technology from 2008, the number of publications related to MLS has grown rapidly [8]. Many urban street area studies based on point cloud data from MLS have been conducted, such as object detection and extraction (e.g., pole-like objects [9]–[12], building facades [13], [14], roads and their boundaries [15]–[19]), scene semantic segmentation and object classification [20]–[23], and high-precision navigation map generation [24]–[26]. All of the abovementioned studies show great potential for individual street trees segmentation and extraction from MLS data.

Some scholars have done lots of researches on the extraction of street trees in urban areas and proposed some methods for individual trees extraction. These methods have better extraction results in simple scenes, especially that without blocked tree trunks. However, for the complex scenes where the tree trunks are blocked by cars and green belts, and the crown touching or interlocking is large, the existing methods have the problems in missing extraction and have low correctness of extraction results. Therefore, this article proposes an individual trees extraction method named “uphill clustering” based on over-segmentation,

Manuscript received October 14, 2020; revised December 23, 2020 and January 3, 2021; accepted January 10, 2021. Date of publication January 14, 2021; date of current version February 8, 2021. This work was supported in part by the National Natural Science Foundation of China under Grant 41974213 and in part by the Beijing Key Laboratory of Urban Spatial Information Engineering under Grant 2020219. (Corresponding author: Jintao Li.)

Jintao Li is with the College of Surveying and Geo-Informatics, Tongji University, Shanghai 200092, China, and also with the Beijing Key Laboratory of Urban Spatial Information Engineering, Beijing 100038, China (e-mail: lijintao@tongji.edu.cn).

Xiaojun Cheng is with the College of Surveying and Geo-Informatics, Tongji University, Shanghai 200092, China (e-mail: cxj@tongji.edu.cn).

Zhenlun Wu is with the Big Data Development Administration of Yichun, Yichun 336000, China (e-mail: yewzl@yichun.gov.cn).

Wang Guo is with the Shanghai Huace Navigation Technology Company Ltd., Shanghai 201702, China (e-mail: wang_guo@huace.cn).

Digital Object Identifier 10.1109/JSTARS.2021.3051653

which aims to realize the automatic extraction and improve the accuracy of the individual trees extraction in urban street areas from MLS data.

The rest of the article is organized as follows. In Section II, related works on individual trees extraction in urban street areas from MLS data are introduced. In Section III, the method for the individual street trees extraction is presented. In Section IV, the experiments and evaluations of the proposed method are conducted with a real dataset. In Section V, the experiment results are discussed in detail. Finally, conclusions are drawn and future work is presented in Section VI.

II. RELATED WORKS

The main process of extracting individual trees from MLS data comprises two steps. First, nontree objects (e.g., ground and building facades) which are easily to identify are removed by the pretreatment [27]. And then, the geometric characteristics of the local structures, such as height [28], point density [29], tree crown radius [30], 3-D structure tensor features [9], shape complexity [31], are used to extract individual trees with trunks and crowns from the remaining objects. According to Vo *et al.* [32] and Li *et al.* [33], the existing methods for individual trees extraction in urban street areas based on MLS data are divided into two categories: region growing-based [28], [31], [33]–[35] and clustering-based methods [30], [36]–[40].

Among the region growing-based methods, the region growing seed points generally located on the trunks should be selected first. And then, the extraction for the whole trees can be accomplished by the growing of the seed points according to certain methods, such as competing region growing algorithm [31], breadth-first search algorithm [34], and dual growing method [33]. It is important to select the seed points correctly to improve the completeness and correctness of the extraction. Yue *et al.* [28] selected seed points on tree trunks based on the elevation difference and density of each grid point. Wu *et al.* [31] selected them according to the area and shape of the voxels projected to the horizontal plane at a relative height of 1.2–1.4 m above the ground. Li *et al.* [33] searched for the seed points on tree trunks according to the rules that a tree trunk stands near the horizontal center of the corresponding crown and has a smaller diameter than the crown with a relatively cylindrical shape. Wu *et al.* [34] pointed that if the plane coordinate of the gravity center of a supervoxel and other points in the supervoxel are close to the detection position, the supervoxel would be more likely to belong to the detection position, which is exactly the seed point on the tree trunk. Similarly, Zhong *et al.* [35] selected seed points according to the local maxima in the horizontal histogram of the octree nodes and their shape characteristics after the construction of the octree. The extraction results of these methods are highly depended on the selection of seed points [41]. For trees whose trunks are not blocked, these methods can completely select the trunk position of each tree, and the corresponding tree can be extracted independently from the trunk position through upward and downward growth. Nevertheless, it is problematic when the tree trunks are blocked by cars and green belts due to the inability of the selection for seed points on the trunks.

Among the clustering-based methods, Huang *et al.* [37] performed Euclidean distance clustering on the points after the ground removed, and extracted individual trees with the support vector machine classifier. Moreover, Guan *et al.* [36] combined the Euclidean distance clustering and voxel-based normalization cut [42] segmentation for the extraction of individual trees. In order to improve the results of individual trees extraction, Weinmann *et al.* [38] extracted independent trees via mean shift clustering and shape analysis. Yadav *et al.* [30] and Xu *et al.* [39] segmented and extracted each crown following the rule that for any point cloud except for the tree vertex, the point belongs to the tree where the nearest tree vertex is located. Xu *et al.* [40] proposed a bottom-up hierarchical clustering method to cluster nonphotosynthetic components of trees, and clustered the leaf regions according to the principle of closest to the clustered nonphotosynthetic components. The existing clustering-based methods can extract individual trees well in some simple scenes where the adjacent street trees have relatively large spacing, less touching, or interlocking with urban infrastructures. However, in the scenes where the street trees have different crown size, the crown touching or interlocking is large, and there is an overlap between tree crowns and other urban infrastructures, these methods demonstrate low identification accuracy and poor crown segmentation results.

In order to overcome the deficiencies of the existing methods, an “uphill clustering” method based on over-segmentation is presented in this article for the automatic extraction of individual trees in urban street areas from MLS data. The main contributions of this article include the following conditions.

- 1) We proposed a new uphill clustering method for individual street trees extraction from MLS data.
- 2) We realized the adaptive setting of clustering threshold parameters, which improved the automation of individual trees extraction.
- 3) We took the point density into account when performing the over-segmentation to improve the supervoxels segmentation method proposed by Lin *et al.* [43] and the improved method shows advantages on the processing of MLS point cloud data with nonuniform densities.

III. METHODOLOGY

MLS point cloud data of urban scenes contains many nontree objects, such as ground, building facades, vertical poles, and cars, which cause difficulties in the extraction of individual street trees. In order to accurately extract each street tree, the proposed method based on uphill clustering mainly includes the following processes. First, we over-segment the original point cloud data to generate supervoxels. This operation can reduce the number of point clouds, improve the computational efficiency, and it can also distinguish the boundaries of different objects well [43]. Second, the typical object structures, such as ground, building facades, low planar structures, horizontal linear structures, and vertical linear structures (potential tree trunks) are all identified after the extraction of planar and linear structures based on the region growing of supervoxels. Then, the remaining volumetric object structures (potential tree crowns) are resegmented and

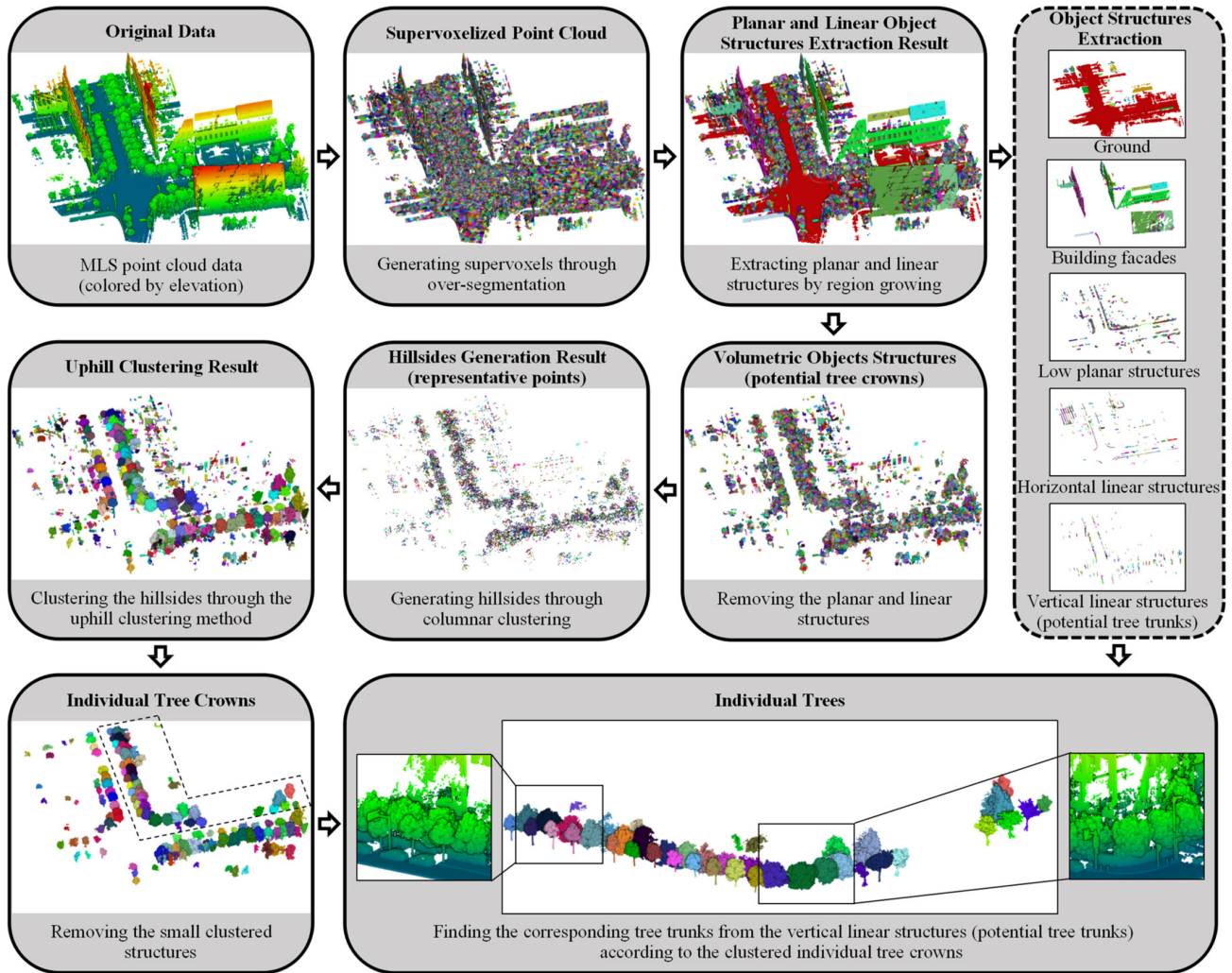


Fig. 1. Overall workflow of the proposed method.

clustered to generate “hillsides,” and the uphill clustering is conducted to segment the potential tree crowns individually. Finally, tree crowns are selected and the corresponding tree trunks are found from the potential trunks. The overall workflow sketch is illustrated in Fig. 1.

A. Supervoxels Generation

Supervoxel can be defined as the 3-D analog of superpixel [44] or a compact point cluster [43]. Using the supervoxels, the number of original 3-D points can be greatly reduced and the processing efficiency will be improved. In addition, a good supervoxel generation method can preserve the object boundaries and provide a natural and compact representation for the original 3-D points, which allows the operations to be performed on a local region with consistent features instead of the original scattered points. Supervoxels have received a lot of attention in 3-D point cloud processing, such as object detection [39], [45], and semantic segmentation or classification [46], [47]. Defined as a compact point cluster as that in reference [43], supervoxels are generate to reduce the amount of data and improve the efficiency of individual trees extraction in this article.

Among the supervoxels generation methods, Papon *et al.* [44] proposed the Voxel Cloud Connectivity Segmentation (VCCS) algorithm, in which the initial supervoxels are formed with the seed points selected uniformly in 3-D space, and then the final supervoxels are generated with local k-means clustering method. The corresponding result depends on the selection of seed points and the setting of the voxel resolution. For the point cloud data with nonuniform density, the object boundaries cannot be ideally preserved, and there exists the deficiency that more than one object may overlap with the same voxel [43]. Thus, Lin *et al.* [43] regarded supervoxel segmentation as a subset selection problem. First, the number of supervoxels, N , or the desired resolution of supervoxels, R (N can be evaluated by R) is specified. Then, N supervoxels are selected by minimizing the sum of the dissimilarity distance (measured by the distance metric, D) between each point and its corresponding representative point. This method is more suitable for the extraction or detection of objects because of its better preservation of object boundaries. However, since only the normal vector difference and Euclidean distance between points are considered in the distance metric, D , the resolutions of supervoxels generated from the areas with different point densities are quite different, which is particularly

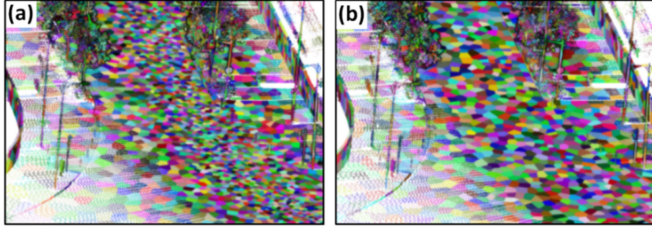


Fig. 2. Supervoxels generation results of MLS data with different point densities. (a) Density inconsistency not considered. (b) Density inconsistency considered.

obvious for MLS point cloud data. As shown in Fig. 2(a), the point cloud is denser on the middle of the road near the laser scanner, so the resolutions of the generated supervoxels are smaller. Along both sides of the road far from the scanner, where the point cloud density is smaller, the corresponding resolutions of the generated supervoxels are larger. Therefore, using this method directly to the extraction of street trees from MLS point cloud data will cause two problems as follows.

- 1) The average resolution of the supervoxels near the tree along both sides of the road is inconsistent with the input desired resolution, R , which makes it difficult to select the parameter, R . R represents the average resolution of generated supervoxels where the point densities are close to the average point density in the original point cloud. The average resolution of supervoxels near the tree on both sides of the road is greater than the desired resolution.
- 2) A large part of the generated supervoxels are distributed on the road, and the number of points cannot be efficiently reduced. The average resolution of the supervoxels on the road is small and the number of supervoxels is large, which can be attributed to the high point density on the road surface for MLS data. However, the road surface is usually a simple flat structure, so there is no need to use too many supervoxels for representation. Therefore, it is necessary to reduce the number of supervoxels on the road.

To solve the two mentioned problems, the distance metric in [43] is improved with the inconsistency of point density considered in this article. Using the improved method, the influence of density inconsistency on the average resolution of generated supervoxels can be avoided as much as possible and the number of supervoxels on the road can be reduced effectively. The optimized distance metric is expressed as

$$D(p, q) = 1 - |n_p \cdot n_q| + \alpha \frac{\|p - q\| - K \cdot M_{\text{dis}} + \text{dis}_{pq}}{R} \quad (1)$$

where n_p and n_q are the normal vectors of the points p and q , which are normalized to the unit length, respectively. The normal vector is calculated as the same as the VCCS implementation in [48]. K is a parameter that needs to be specified to control the influence of point density. M_{dis} represents the average point density of all points in the original point cloud, which is expressed by the average point spacing. dis_{pq} is the average density at point p and q , which is represented by the average point spacing at point p and point q . In practice, the point spacing at point p is represented by the average of the distances from point p to the

points in its k -nearest neighborhood. α is the weight parameter to balance the influence of normal vector difference and spatial distance. In practice, α is taken as 0.4, which is the same as that in [43] and [48].

The supervoxels generated with the same desired resolution by the distance metric before and after optimization are shown in Fig. 2(a) and (b), respectively. From the comparison in Fig. 2, we can see that the resolutions of the supervoxels generated with the point density considered are more uniform, which facilitates the selection of the desired resolution, R . Moreover, the number of supervoxels on the road is greatly reduced, which effectively reduced the amount of data by using supervoxels to represent the original points.

B. Planar and Linear Object Structures Extraction

After supervoxels are generated, all points can correspond to the supervoxels which they belong to. Almost all points in the same supervoxel belong to the same object or part of the same object. This provides a good foundation for the detection of objects. Since we focus on the extraction of individual trees, we first extract the typical planar and linear object structures based on the region growing of supervoxels, and then remove the typical nontree planar and linear object structures.

Using principal component analysis method, the geometric structures for each supervoxel are calculated as follows [49], [50].

Let p_i ($i = 1, 2, \dots, k$) be the points in one supervoxel. The covariance matrix \mathbf{M} of them can be written as

$$\mathbf{M} = \frac{1}{k} \sum_{i=1}^k (p_i - \bar{p}) \cdot (p_i - \bar{p})^T \quad (2)$$

where k is the number of points in the supervoxel, \bar{p} is the centroid of the supervoxel, and $\bar{p} = \frac{1}{k} \sum_{i=1}^k p_i$.

The eigenvalues $\lambda_1, \lambda_2, \lambda_3$; ($\lambda_1 \geq \lambda_2 \geq \lambda_3$) of \mathbf{M} can be determined, and they represent the 3-D geometric tensor features of the supervoxel.

Different from Yang *et al.* [50], which used probabilistic methods to determine whether a supervoxel belongs to a linear, planar, or volumetric structure, we determine the geometric structure, V_L , of the supervoxel according to the three eigenvalues of \mathbf{M} by specifying parameter thresholds K_L and K_P . This can effectively avoid salt-and-pepper noise during the subsequent region growing process. The method of judging the geometric structures of supervoxels is as follows:

$$V_{Lis} : \begin{cases} \text{linear,} & \text{if } \lambda_1 \geq K_L \cdot \lambda_2 \\ \text{planar,} & \text{else if } \lambda_2 \geq K_P \cdot \lambda_3 \\ \text{volumetric,} & \text{else} \end{cases} \quad (3)$$

For the supervoxels with planar and linear structures, their normal direction, V_N , and principal direction, V_P , are calculated respectively. V_N and V_P are the corresponding eigenvectors to the smallest and largest eigenvalue of \mathbf{M} .

With the geometric characteristics of supervoxels, all points can be represented by N supervoxel representative points with geometric characteristics (linear, planar, or volumetric structure categories, normal directions of planar structures or principal directions of linear structures). The planar and linear

TABLE I
SEVERAL TYPICAL URBAN OBJECT STRUCTURES AND THEIR CORRESPONDING JUDGMENT METHODS

Structures	Descriptions	Judgment methods
Ground	A ground can be regarded as a horizontal plane with an area greater than a certain threshold.	The product of the length and width of the minimum bounding box is greater than the threshold, T_{GA} , and the angle between the normal direction and the Z axis is less than the threshold, T_{GN} .
Building facades	A building facade can be regarded as a vertical plane with an area greater than a certain threshold.	The product of the length and height of the minimum bounding box is greater than the threshold, T_{BA} , and the angle between the normal direction and the horizontal plane is less than the threshold, T_{BN} .
Low planar structures	A low planar structure can be regarded as a plane whose area is greater than a certain threshold and the distance between the highest point and the ground is less than a certain height.	The length of the minimum bounding box is greater than the threshold, T_{LPL} , the width or height is greater than the threshold, T_{LPW} ; and the height between the highest point of the structure and the ground is less than the threshold, T_{LPH} .
Horizontal linear structures	A horizontal linear structure can be regarded as a linear structure with a certain length and parallel to the ground.	The length of the minimum bounding box is greater than the threshold, T_{HLL} , and the angle between the principal direction and the horizontal plane is less than the threshold, T_{HLP} .
Vertical linear structures (potential tree trunks)	A vertical linear structure can be regarded as a linear structure with a certain length and perpendicular to the ground.	The height of the minimum bounding box is greater than the threshold, T_{VLL} , and the angle between the principal direction and the Z axis is less than the threshold, T_{VLP} .

object structures are detected successively with region growing method. The process is as follows.

- 1) Detection of planar object structures. The threshold parameters $K_L = 10$ and $K_P = 5$ are used to calculate the supervoxels geometric structures in the detection of the planar object structures. Then, the first seed supervoxel is randomly selected from the planar supervoxels, and the spatially adjacent supervoxels are regarded as the candidate growing supervoxels. The growth criterion is that the angle of normal vector between the supervoxel and the seed supervoxel is smaller than the threshold, T_N ($T_N = 20^\circ$ in practice). The supervoxels that satisfy the growth criterion are clustered into the seed supervoxel, and their neighborhoods are putted into the candidate growing supervoxels. For the candidate supervoxels, the growing process is carried out with the growth criterion, until the detection of the planar object structure of the first seed supervoxel is achieved. After the growth of the planar object structure where the first seed supervoxel is located, the next seed supervoxel is selected to start the growth of the next planar structure until the detections for all the planar object structures are completed.
- 2) Detection of linear object structures. The geometric structures of the grown planar object structures are recalculated with threshold parameters $K_L = 5$, $K_P = 10$, and the recalculated planar object structures are used together with other ungrown linear supervoxels for linear object structures detection. The detection method of linear object structures is similar to that of planar object structures, except for that the growth criterion is replaced by the criterion that the angle of principal direction between the supervoxel and the seed supervoxel is less than the threshold, T_P ($T_P = 20^\circ$ in practice).

The planar and linear object structures generated after the region growing and the ungrown supervoxels are all parts of objects. For convenience, we call them object structures. Among

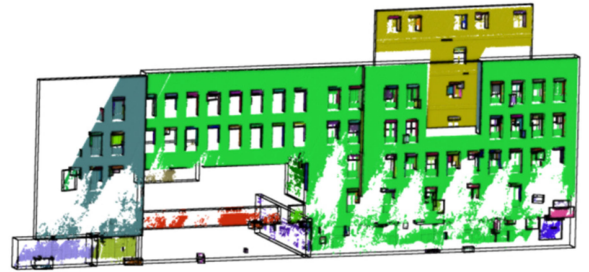


Fig. 3. Extracted building facade structures.

them, several typical object structures including ground, building facades, low vegetation in the shape of a plane, horizontal linear structures such as roadsides, linear structures of buildings, and vertical linear structures such as traffic sign poles, street light poles, and tree trunks can be easily extracted. The vertical linear structures of these typical object structures are potential tree trunks. The structures other than the above typical object structures belong to the potential tree crowns. Inspired by Yang *et al.* [50], we extract the typical object structures according to their minimum bounding box size and their geometric characteristics. And then, other typical object structures except for the potential tree trunk and crown structures are removed. The judgment method of each typical object structure is shown in Table I.

In addition to the large planar structures, the building facades also contain many other small structures, such as door and window frames, air conditioners. Therefore, after the building facade structures are extracted according to the judgment method in Table I, other structures located within the extracted minimum bounding boxes of the building facades are also regarded as the building facade structures, as shown in Fig. 3. In the same way, for the low planar structures, other structures located in the smallest bounding boxes of the low planar structures are also regarded as the low planar structures.

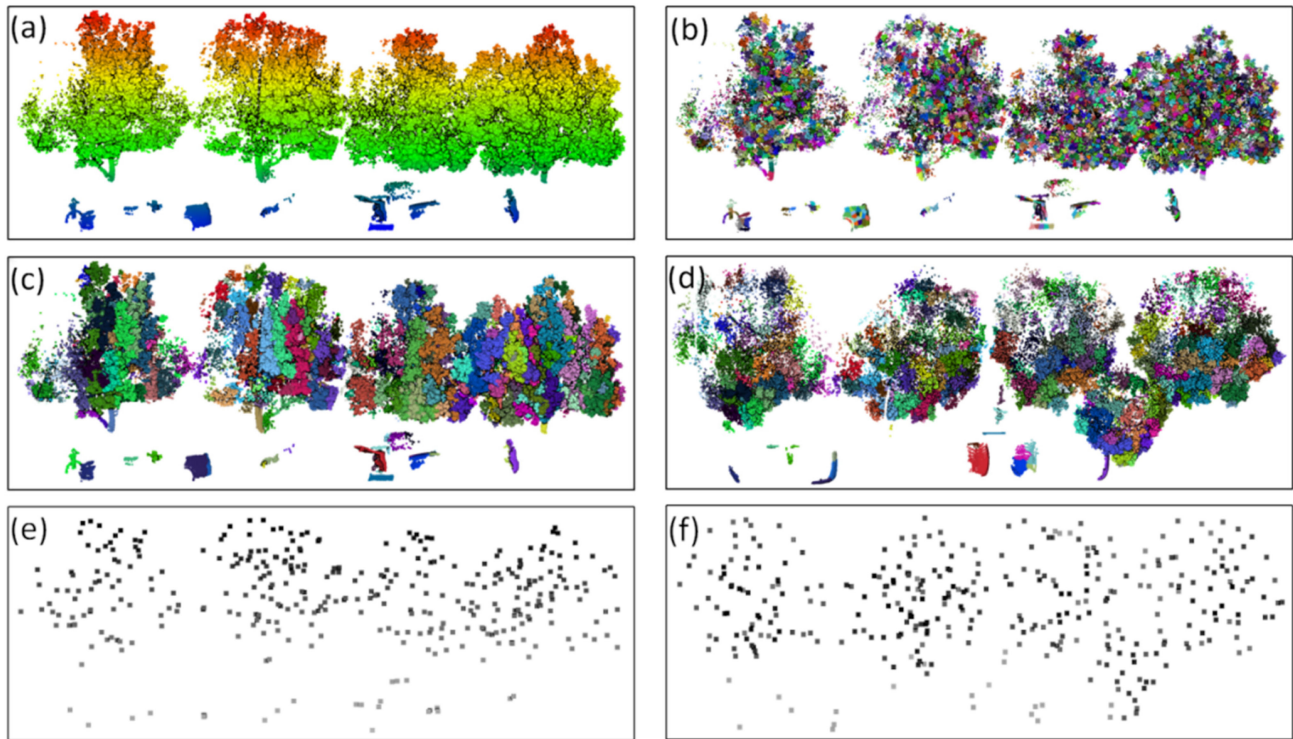


Fig. 4. Hillside generation process. (a) Volumetric geometric points (colored by elevation). (b) Supervoxels. (c) Side view of the hillside structure. (d) Top view of the hillside structure. (e) Side view of representative points of the hillside structure. (f) Top view of representative points of the hillside structure.

C. Hillside Generation

After planar and linear object structures detection and extraction, typical object structures, such as ground, building facades, roadsides, street light poles, and tree trunks, have been extracted. The rest of the object structures are mainly tree crown object structures and other noncrown small object structures, as shown in volumetric object structures in Fig. 1. Compared with tree crowns, these noncrown objects are usually smaller and separated from each other in space [Fig. 4(a)], so they can be distinguished from the tree crowns by clustering. However, there may be touching or interlocking between the crowns of adjacent trees. Therefore, existing clustering methods such as Euclidean distance clustering and mean shift clustering are difficult to separate each tree crown. To this end, we first generate “hillsides” for uphill clustering by reover-segmentation and columnar clustering of the volumetric object structures. And then we achieve independent segmentation of the tree crowns through uphill clustering.

When generating supervoxels from the original point cloud, we use (1) as the distance metric function, and the normal vector consistency is considered in the distance metric function D . But for tree crowns, the points of the crowns usually appear as scattered points with volumetric structures, and the normal vectors of the two points are quite different even if they are adjacent. The shape of the supervoxel generated by considering the consistency of the normal vector is extremely irregular and the points of two tree crowns may be distributed in the same supervoxel. Independent extraction of tree crowns directly based

on the original supervoxels easily leads to poor extraction of adjacent tree crowns. Therefore, before the independent segmentation of the crowns, we reover-segment the point cloud in the volumetric object structures to generate new supervoxels with the desired resolution R_{cro} , in which the spatial Euclidean distance is considered only in the distance metric D_{cro} .

$$D_{cro}(p, q) = \|p - q\|. \quad (4)$$

Only considering the spatial Euclidean distance can better distinguish the tree crown boundaries while reducing the number of points. The regenerated supervoxels are shown in Fig. 4(b).

The result of reover-segmentation is further applied to columnar clustering to generate “hillside” for uphill clustering [Fig. 4(c) and (d)]. The implementation of columnar clustering is similar to the supervoxels generation, which is also regarded as a subset selection problem. The supervoxels whose distance in the XY plane is less than the threshold R_{col} are merged. The plane distance in the XY plane is used only in the columnar clustering distance metric D_{col} .

For each columnar cluster in the “hillside,” we use the highest point as a representative point to represent it. The side view and top view of the “hillside” represented by representative points are shown in Fig. 4(e) and (f), respectively. Using the highest point as the representative point can make the columnar cluster of the same tree clustered together more closely with the tree apex as the center and increase the distance between different crowns, which facilitates the individual extraction of different crowns.

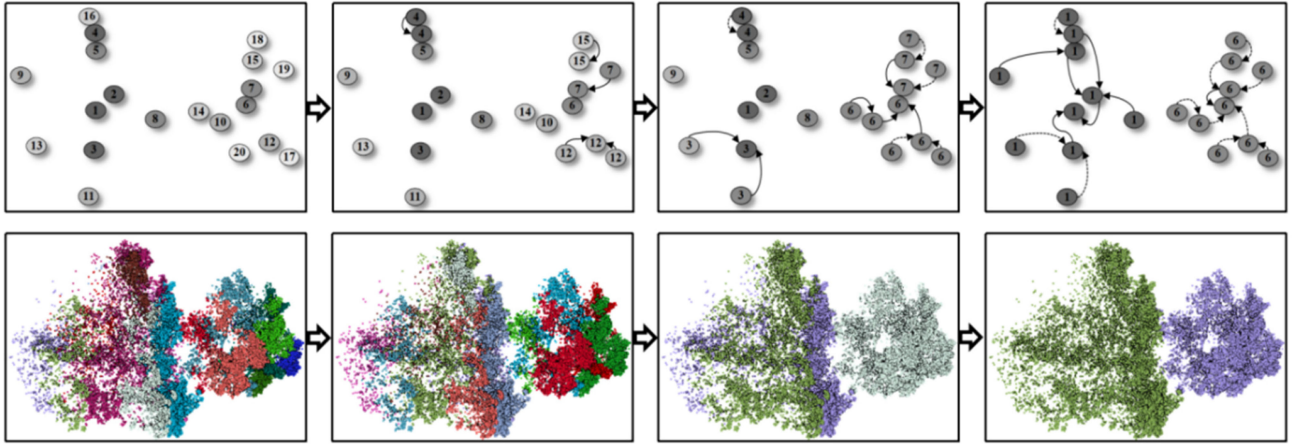


Fig. 5. Uphill clustering process. Upper, clustering process of the representative points (numbered and colored by elevation), top view; lower, columnar clusters corresponding to clustering process of the representative points, side view.

D. Uphill Clustering

For the representative points of the generated hillside structure, the clustering category to which each representative point and its corresponding columnar cluster belong is determined in the order of height from low to high with the uphill clustering criterion, so as to realize the individual extraction of the tree crowns. Fig. 5 shows the hillside clustering process of the representative points and their corresponding original points. The specific clustering process is as follows.

- 1) For the representative points of the columnar clusters in the hillside structure, we sort them according to their elevation and number them sequentially. The number represents the cluster category to which the columnar cluster belongs. Before the uphill clustering, the number of cluster categories is equal to the number of columnar clusters.
- 2) According to the order of the height from low to high, that is, the number from large to small, we cluster each representative point P_i in the hillside structure in turn. Next, we find the representative point P_j that is closest to P_i in the XY plane and whose number is less than P_i (that is, higher than P_i in spatial). Determine whether P_i and P_j meet the clustering condition, that is, whether they are adjacent in space and the distance in the XY plane is less than the threshold T_c . If the clustering conditions are met, the representative points P_i and P_j belong to the same cluster category. And then the numbers of the representative points P_i and representative points with the same numbers as P_i (that is, the columnar clusters belong to the cluster category of P_i) are both changed to the number of P_j .
- 3) After the clustering of the highest representative point is completed, all representative points of the columnar clusters on the hillside structure have their corresponding cluster category numbers. The columnar clusters with the same number belong to the same clustering category, and the columnar clusters with different numbers can be distinguished, so as to realize the uphill clustering.

For the clustering results of the hillside structure, the spatial minimum bounding box of each cluster is calculated, and the

cluster with the size of the minimum bounding box greater than the threshold S_{bb} is regarded as the tree crowns, as the individual tree crowns shown in Fig. 1. After the crown of each tree is extracted, the plane coordinates of the highest point of each crown are used to indicate the position of the crown in XY plane. The nearest vertical linear structure whose distance to the crown in XY plane is less than D_{ct} is selected as the corresponding tree trunk from the potential tree trunk structures. The tree crown has no corresponding trunk if it does not have a potential trunk structure within a distance less than D_{ct} in the XY plane. So far, individual extraction of street trees from MLS point cloud data in urban areas has been completed, which is shown in Fig. 1, individual trees part.

To improve the self-adaptive ability of the uphill clustering method for extracting crowns of different sizes, the selection of the clustering threshold T_c adopts an adaptive method according to the size of the tree crown in the process of clustering representative points of the columnar cluster. Assuming that the crown width is proportional to the crown length, the clustering threshold T_c can be adaptively selected according to the current length, H_i , of the columnar cluster.

$$T_c = \begin{cases} \frac{1}{3}H_i \cdot R_c, & H_i \geq H_t \\ \frac{1}{3}H_t \cdot R_c, & H_i < H_t \end{cases} \quad (5)$$

where R_c is the ratio of crown width to crown length, and its value can be selected according to the tree species; H_t is the length threshold of columnar clusters. In the uphill clustering process, the use of H_t can avoid clustering failures of columnar cluster whose length is less than H_t .

The method with fixed thresholds has the shortcoming that it is difficult to accurately extract tree crowns of different sizes, which can be avoided by the adaptive clustering threshold method. As shown in Fig. 6, A, B, C, and D are four representative points. For the clustering of D, the searched nearest neighbor representative point is B, and the condition for that the columnar clusters in D can be clustered into B is that d_{BD} is less than the threshold T_{cD} . For the clustering of C, the searched nearest neighbor representative point is A, and the corresponding clustering condition is that d_{AC} is less than the threshold T_{cC} .

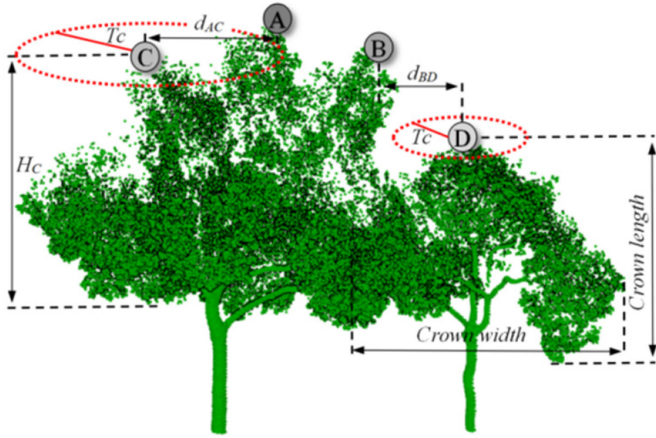


Fig. 6. Schematic diagram of adaptive selection of clustering threshold according to the length of columnar clusters.

Since d_{AC} is greater than d_{BD} , when the fixed threshold T_c is small, the two columnar clusters A and C will be divided into two cluster categories, resulting in over-segmentation of the tree crowns; when the fixed threshold T_c is large, B and D will be clustered into the same cluster category, resulting in under-segmentation. The adaptive threshold selection method adopted in this article can automatically determine the size of the threshold T_c according to the length of the current columnar cluster, so that the clustering threshold T_{cD} at representative point D is smaller than the clustering threshold T_{cC} at representative point C . In this way, the shortcomings of fixed threshold that it is difficult to cluster spatially connected and different-sized tree crowns can be effectively avoided.

IV. EXPERIMENTS AND EVALUATIONS

A. Test Data

The data shown in Fig. 7(a) is used to verify the individual trees extraction method proposed in this article. The data was collected by an MLS system in an urban street, with a total of 10 738 632 original measurement points. The length of the road in the experimental data is about 220 m, and the height difference between the two ends of the road is about 0.5 m. There is a total of 129 trees that can be artificially identified from the scanning data, of which 85 are street trees on both sides of the road and 44 are greening trees in the green belt areas. The size, height, density, and tree species of the street trees are different. The trunks of some trees are blocked by cars parked on the roadside and the green belt walls under the trees [Fig. 7(b)]. In addition, the poles contained in the street trees such as traffic sign poles, street light poles [Fig. 7(c)], and bicycles parked under the street trees [Fig. 7(c)] all have influence on the extraction of individual trees. The point density of trees in the green belt areas is sparse and the density difference is large [Fig. 7(d)] because the greening trees are far away from the scanner and are seriously blocked. In addition, some greening trees are close to the building [Fig. 7(e)]. All of the above characteristics lead to the difficulties in the extraction of individual trees.

In order to show the close-view of the extraction results and analyze the applicability of the proposed method in scenes with different complexity, we divided the trees into six small regions and numbered them with 1–6 [Fig. 7(a)]. The trees in region 1 and 6 are located in green belt areas and belong to greening trees. The trunks of greening trees are usually not obvious, and the height under branches is usually small, so it is difficult to effectively extract the trees by identifying the tree trunks and then growing from them. The trees in regions 2–5 belong to street trees, which are the main objects the proposed method focus on. Among them, the environmental complexity of each region is different. Except for cars, bicycles, street lights, and traffic signs in region 4, the street trees in this region are in two parallel rows. The distance between the street trees is close, the crowns are connected, and the tree height and the crown size vary greatly. In addition, the trunks of the second row of trees far from the scanner are seriously blocked by the green belt walls [Fig. 7(b)]. Therefore, region 4 is the most complex for individual trees extraction. It should be noted that it also contains some greening trees, but it is difficult to distinguish them from the scanning data due to severe block. Therefore, in the experimental part, for the trees in region 4, we only considered the two rows of street trees close to the road that can be artificially identified from the scanning data. The experimental data used here contains six small regions with different environmental complexity, which can effectively verify the feasibility of the proposed method for individual trees extraction.

B. Individual Trees Extraction Results

The method proposed in this article is used to extract individual trees from the experimental data. When supervoxel segmentation is performed on the original point cloud data, the desired resolution of the supervoxel R is taken as 1.0 m, and the parameter K is taken as 6. When extracting several typical object structures using the judgment methods described in Table I, we set the empirical parameter thresholds as follows: $T_{GA} = T_{BA} = 20 \text{ m}^2$, $T_{GN} = T_{HLP} = T_{VLP} = 20^\circ$, $T_{BN} = 10^\circ$, $T_{LPL} = T_{LPW} = 1.5 \text{ m}$, $T_{LPH} = 2.0 \text{ m}$, $T_{HLL} = T_{VLH} = 1.0 \text{ m}$. And the extraction results are shown in Fig. 8. In detail, Fig. 8(a) shows the extraction results of several typical planar and linear object structures not belonging to tree crowns and trunks. Fig. 8(b) shows the extraction results of potential tree trunks, including vertical pole-like structures such as tree trunks, street light poles, and traffic sign poles. Fig. 8(c) shows the remaining potential tree crowns after removing several typical object structures that are not tree crowns from the original data.

After hillside generation and uphill clustering, the potential tree crowns [Fig. 8(c)] are segmented independently. Then, independent tree crowns are extracted from the potential tree crowns according to the size of their minimum bounding boxes and the trunk corresponding to each tree crown is selected (if the corresponding trunk exists) from the potential tree trunks [Fig. 8(b)]. The parameters and thresholds that are adopted in this process are as follows: $R_{cro} = 0.25 \text{ m}$, $R_{col} = 0.5 \text{ m}$, $R_c = 1.5 \text{ m}$, $H_t = 2 \text{ m}$, $S_{bb} = 2 \text{ m} \times 2 \text{ m} \times 2 \text{ m}$, $D_{ct} = 1.0 \text{ m}$. The final individual trees extraction results are shown in Fig. 9,

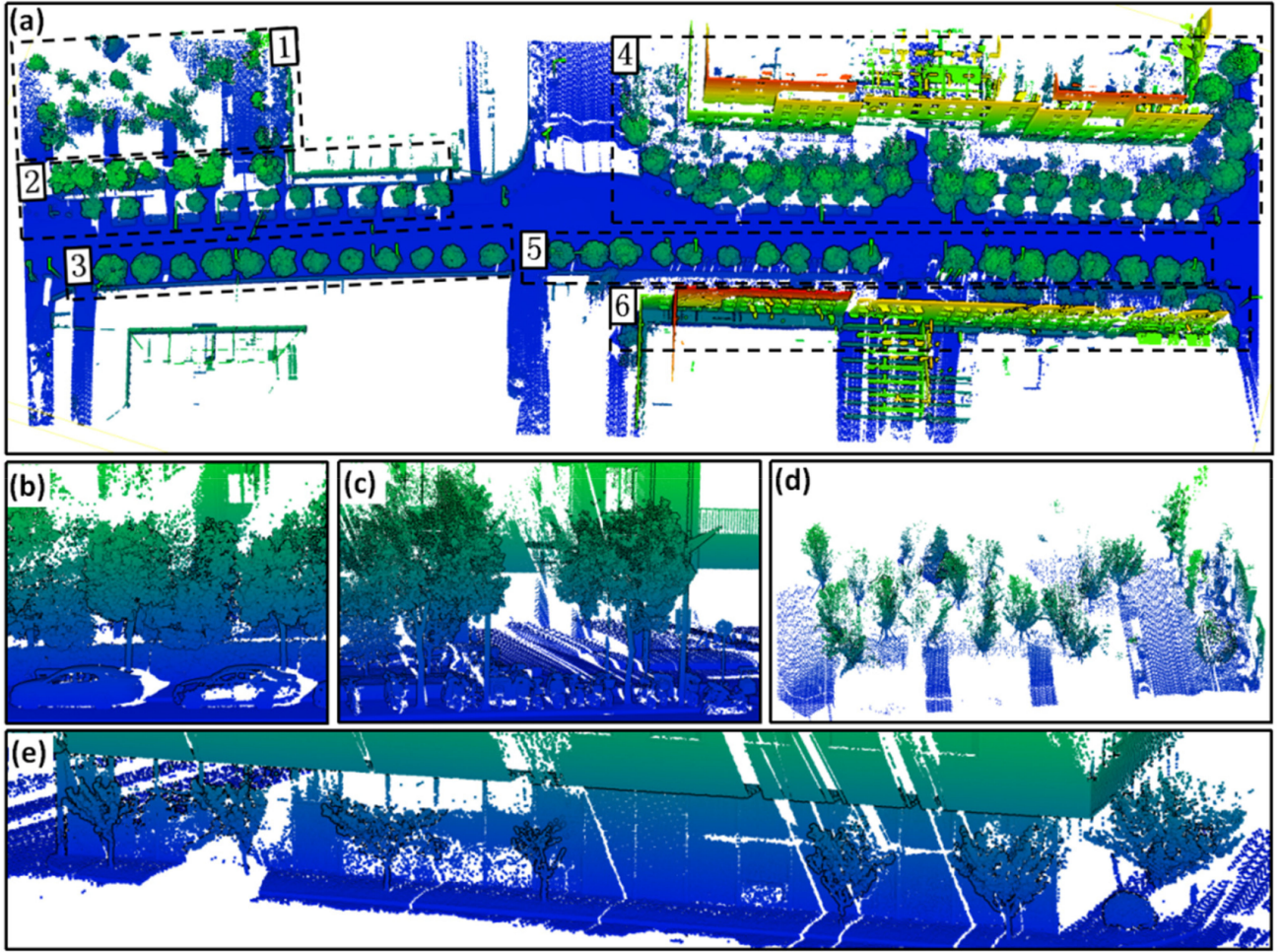


Fig. 7. Test data. (a) Original point cloud and the regions division (colored by elevation). (b)–(e) Close-view of the test data.

with regions 1 and 6 displaying the result of extracted individual greening trees, and regions 2–5 showing that of the street trees.

In order to quantitatively evaluate the results of the individual trees extraction, we calculate the correctness r , completeness p , and F -score f as

$$r = \frac{TP}{TP + FP}, p = \frac{TP}{TP + FN}, f = \frac{2 \times TP}{2 \times TP + FP + FN} \quad (6)$$

TP: the number of trees correctly extracted; FP: the number of trees wrongly extracted; FN: the number of trees that have not been extracted.

The correctness represents the ratio of the number of trees correctly extracted to the number of trees extracted in the experiment, which is used to describe the accuracy of individual trees extraction; the completeness represents the percentage of the number of trees correctly extracted to the total number of trees in the test region, which is used to describe the integrity of the individual trees extraction; F -score is the harmonic mean of correctness and completeness, which is the comprehensive evaluation index of the above two indexes, and can evaluate the comprehensive effect of individual trees extraction. The evaluation of our performance on each region is shown in Table II.

V. DISCUSSION

A. Performance of the Supervoxels Generation

In order to verify the effectiveness of the improved supervoxels generation method with the inconsistency of point density considered, we calculated the relationship between the number of supervoxels on the road surface and the parameter K , and the relationship between the average resolution of the supervoxels and the parameter K , as shown in Fig. 10(a) and (b), respectively. Fig. 11 shows the supervoxels generation results on the road with several different values of K . In Figs. 10 and 11, when $K = 0$, the number of supervoxels on the road is 10 233, and the average resolution of supervoxels on the road is 0.452 m. These are the results in which the inconsistency of point density is not considered. When $K = 0$, the average resolution of supervoxels on the road is much smaller than the average resolution of all supervoxels (1.0 m), so the average resolution of other nonroad supervoxels is about 1.548 m (greater than the average resolution 1.0 m). It can be seen from Figs. 10(b) and 11 that when the inconsistency of point density is considered, the average resolution of supervoxels on the road shows an increasing trend on the whole, and keeps close to 1.0 m with the increase of K . Therefore, the average resolution of nonroad supervoxels

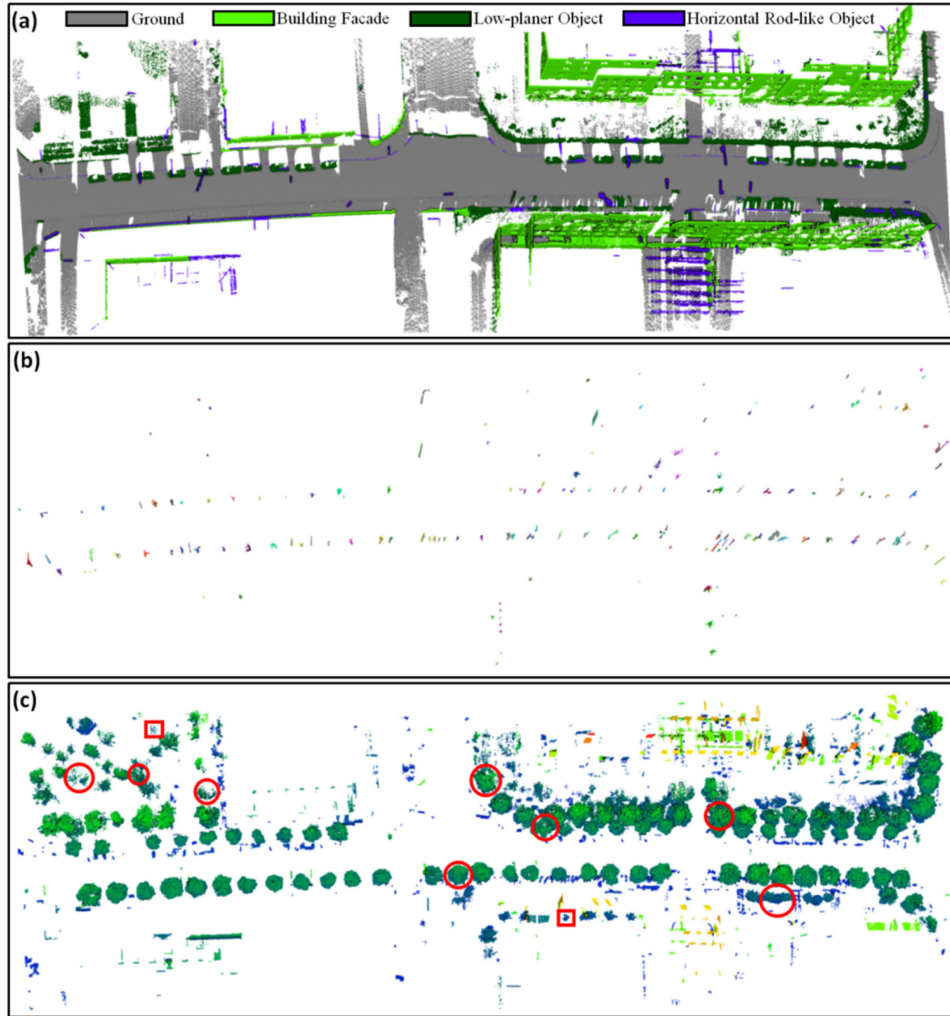


Fig. 8. Object structures extraction. (a) Several typical planar and linear object structures not belonging to tree crowns and trunks. (b) Potential tree trunks (vertical pole-like objects). (c) Potential tree crowns (volumetric object structures).

TABLE II
EVALUATION OF THE EXTRACTED INDIVIDUAL TREES

Region	Reference	TP	FN	FP	r (%)	p (%)	f
1	24	20	1	3	87.0	95.2	0.91
2	17	17	0	0	100	100	1.00
3	12	12	0	0	100	100	1.00
4	38	35	0	3	92.1	100	0.96
5	18	17	0	1	94.4	100	0.97
6	20	15	1	4	78.9	93.8	0.86
Greening trees (1、6)	44	35	2	7	83.3	94.6	0.89
Street trees(2、3、4、5)	85	81	0	4	96.4	100	0.98
Total	129	116	2	11	91.3	98.3	0.95

becomes smaller toward the desired value of 1.0 m. In addition, with the increase of K , the number of supervoxels on the road shows a decreasing trend as a whole [Fig. 10(a)], and the average resolution of supervoxels is more uniform (Fig. 11). Therefore, the supervoxels generation method which considers the inconsistency of point density by selecting the appropriate K cannot

only effectively solve the problem of excessive differences in the average resolution of all supervoxels, but also reduce the number of supervoxels on the road and improve the efficiency of data processing. Combined with Fig. 2, it is proved that considering the inconsistency of point density is of great significance in supervoxels generation.

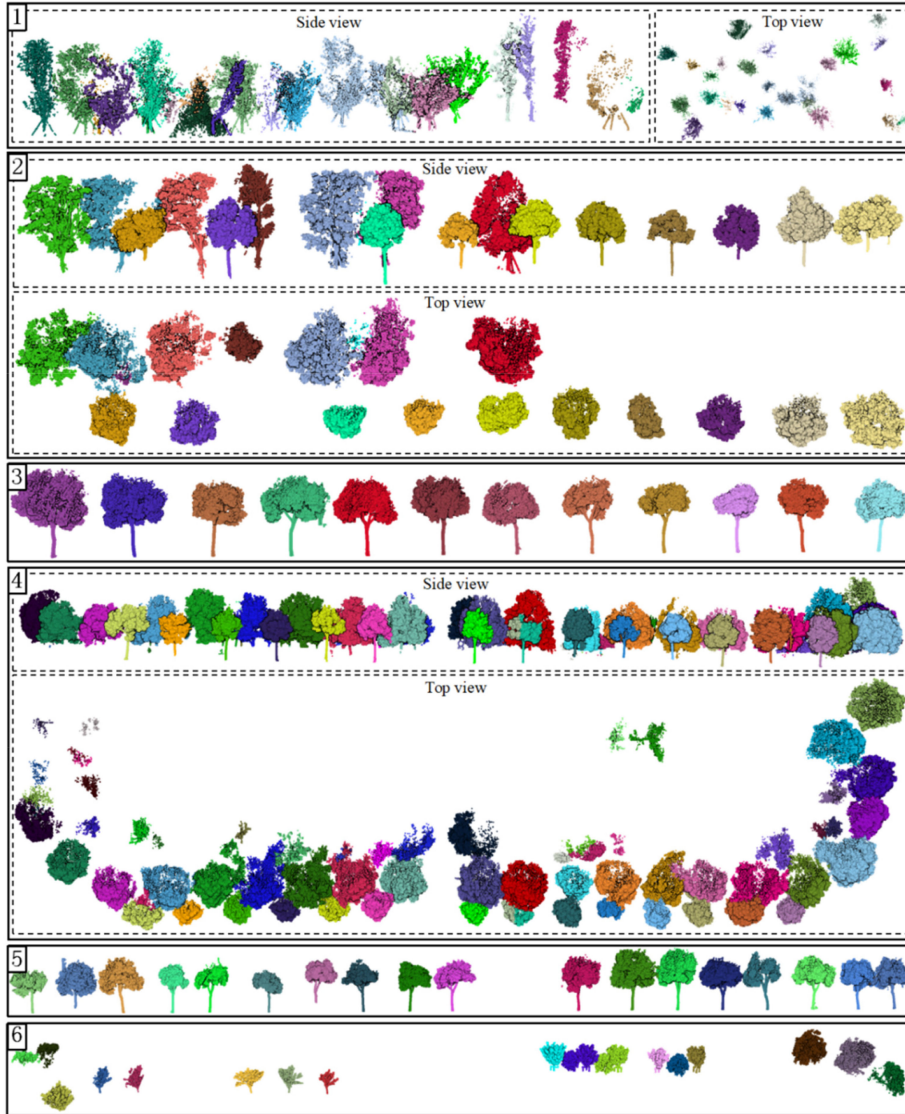


Fig. 9. Close-view of our performance on regions 1–6.

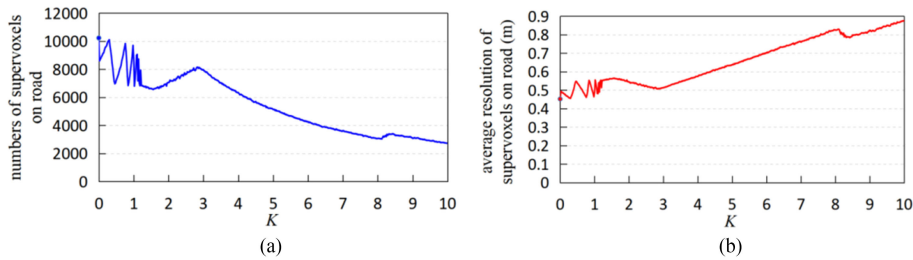


Fig. 10. Relationship between the changes of generated supervoxels on the road and the parameter K . (a) Relationship between the number of supervoxels on the road and the parameter K . (b) Relationship between the average resolution of supervoxels on the road and the parameter K .

B. Performance of the Typical Object Structures Extraction

It can be seen from Fig. 8(a) that the proposed supervoxel-based planar and linear nontree object structures detection method can effectively extract the nontree objects structures like ground, building facades, low planar object structures, and

horizontal pole-like structures. Potential tree trunks (vertical pole-like structures) can also be extracted effectively [Fig. 8(b)]. It can be seen from the potential tree crowns [Fig. 8(c)] that although there are many nontree crown object structures in the potential tree crowns, the tree crowns are reserved without any omission, which provides a guarantee for the completeness of

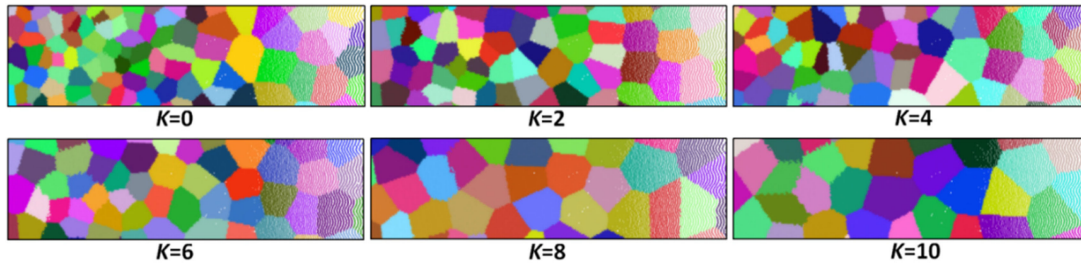


Fig. 11. Supervoxels generation results on the road with different values of K .

crowns extraction in the subsequent processing. Moreover, in the potential tree crowns, the crowns and noncrown structures are not connected with each other and the size of the former is larger. Therefore, the tree crowns and noncrown structures can be distinguished by clustering, which ensures the correctness of independent extraction of the crowns in subsequent processing. In summary, the extraction of typical object structures based on the region growing of supervoxels provides a basis for individual trees extraction.

C. Performance of the Individual Trees Extraction

From the close-view of the individual trees extraction results (Fig. 9), it can be seen that the proposed method has a good extraction result for street trees and greening trees. And for region 4 where trees are dense, the tree crown size is different and some tree trunks are blocked, the proposed method can also extract individual tree well. Fig. 12 shows the extraction results of street trees in several different environments. It can be seen that the proposed method cannot only extract the street trees from simple environments [Fig. 12(a) and (b)] but also can correctly extract trees from complex environments where the tree trunks are blocked severely by cars and green belts and the crown touching or interlocking is large [Fig. 12(c) and (d)].

It can be seen from Table II that the completeness of the proposed method for the extraction of street trees in regions 2–5 has reached 100%, that is, there is no missing extraction, and the correctness is 96.4%. There are four wrongly extracted street trees, which are located in the red circles in Fig. 8, and their close-up views are shown in Fig. 13(a), (b), (c), and (f), respectively. From the close-up view, the wrongly extracted street trees include two types: 1) the tree mixed with other objects like traffic signs [Fig. 13(a) and (c)], resulting from the fact that the tree crown is connected with the other objects; 2) the tree whose crown is wrongly divided into more than one parts [Fig. 13(b) and (f)], which is caused by the incomplete crown or the large difference of point cloud density in the crown.

From the results of trees extraction in regions 1 and 6 in Table II, the proposed method also performs well for the extraction of greening trees in different shapes, and the completeness and correctness are 94.6% and 83.3%, respectively. There are two missing greening trees in the extraction results, which are located in the red rectangles in Fig. 8 and their close-views are shown in Fig. 14. The reason why the tree shown in Fig. 14(a) is missed is that the point spacing of the

tree is larger than the distance recognition threshold, because it is far away from the scanner and blocked severely. The corresponding reason for the missed tree in Fig. 14(b) is that the size of the tree is smaller than the $2\text{ m} \times 2\text{ m} \times 2\text{ m}$ crown recognition thresholds set in our experiment. There are seven trees extracted wrongly in the green belt areas, which are located in the red circles in Fig. 8. Their close-views are shown in Fig. 13(d), (e), (g), and (h), respectively. The reason why the trees shown in Fig. 13(d), (e), and (g) are not correctly extracted is that the tree point cloud is incomplete due to the block. The corresponding reason for Fig. 13(h) is that the distances between trees are too close and the crown touching and interlocking are severe, which causes the two adjacent trees to be wrongly identified as one.

In order to verify the advantages of the proposed method, our performance is compared with other individual street trees extraction methods based on MLS point cloud data, including Wu2013 [31], Wu2016 [34], Li2016 [33], Zhong2017 [35], Huang2015 [37], Yadav2018 [30], Xu2018 [40], and Improved Wu2013. Among them, Wu2013 is a representative region growing-based method, and Improved Wu2013 is the optimized method of Wu2013 to compare the proposed method with the region growing-based method on the same test data. Compared with Wu2013, the condition that the compactness index of crown after region growing is less than 0.5 is added in Improved Wu2013. The calculation of compactness index can be found in [31]. The addition of the compactness index condition can effectively overcome the weakness that the crown without a trunk and the crown with a trunk touched to it may be divided into the same one during the horizontal growth of the crown. This can improve the correctness of individual tree extraction.

Table III shows a description of the datasets and test scenes in the mentioned methods for individual trees extraction. The Improved Wu2013 and the proposed method use the same dataset, which is the experimental data used in this article. Among the 85 street trees in the experimental data, the Improved Wu2013 method extracted 63 street trees (85 with the proposed method), of which 62 were correctly extracted (81 with the proposed method). Because the trunks of some street trees in region 4 are blocked by the low green belts, 22 street trees have not been extracted in the results of the Improved Wu2013 method (there is no missing extraction with the proposed method). The partial comparison of results for the two methods is shown in Fig. 15, which shows that the Improved Wu2013 method cannot extract the street trees with trunks blocked because the trunk seed points

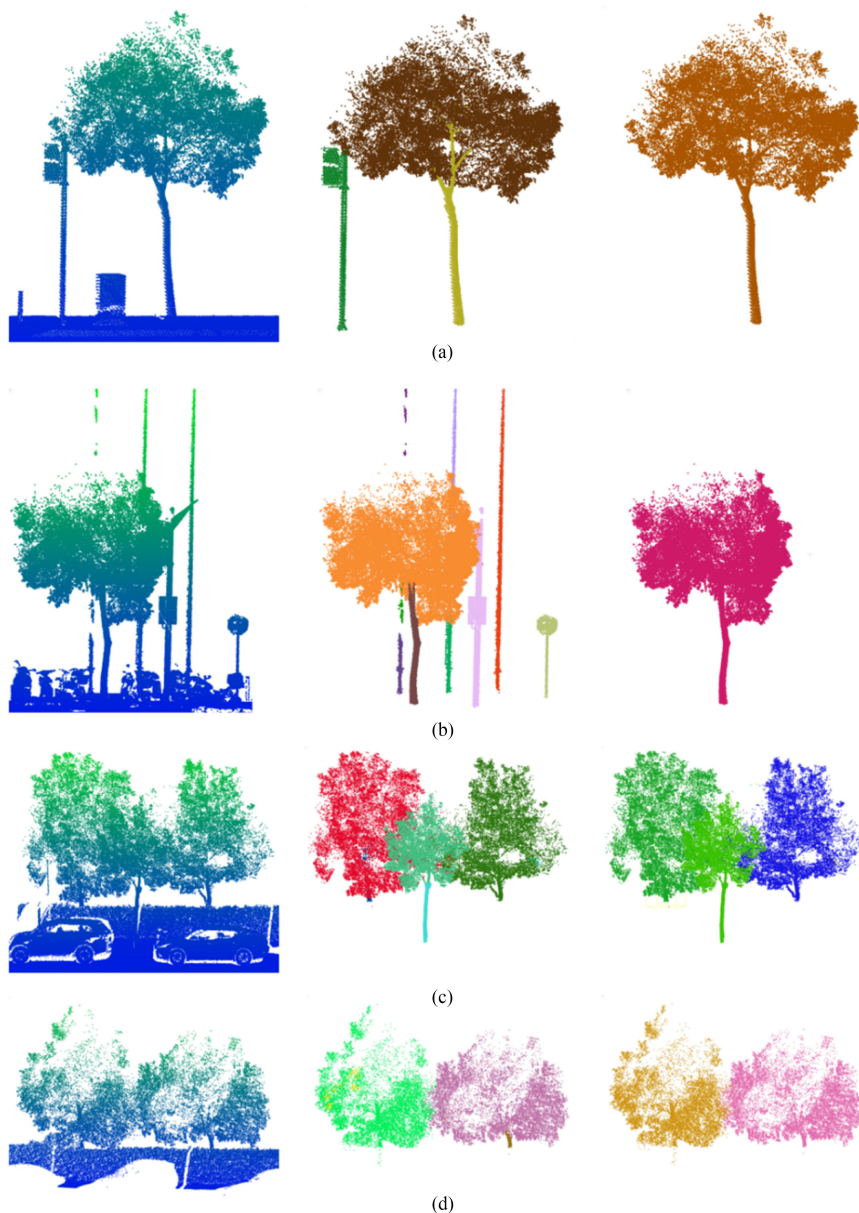


Fig. 12. Extraction results of individual street trees in environments with different complexity. Left: original point cloud data; Middle: tree crowns and potential tree trunks; Right: individual trees with crowns and trunks.

TABLE III
DESCRIPTION OF METHODS AND TEST SCENES IN INDIVIDUAL STREET TREES DETECTION FOR MLS DATA

Algorithms	Individual trees detection method	Density of dataset (points/m ²)	Test scene		
			Environment	Type of trees	Number of trees
Wu2013_1	region growing-based	212	residential area	planetree	72
Wu2013_2	region growing-based	224	residential area	camphortree	68
Wu2016	region growing-based	—	urban area	palmtree	311
Li2016_1	region growing-based	123	urban area	mixed	66
Li2016_2	region growing-based	306	urban area	mixed	29
Zhong2017	region growing-based	222	urban area	mixed	—
Huang2015	cluster-based	—	urban area	mixed	123
Yadav2018	cluster-based	1240	urban area	palmtree	17
Xu2018	cluster-based	700	urban area	mixed	182
Improved Wu2013	region growing-based	456	urban area	mixed	85
Proposed	cluster-based	456	urban area	mixed	85

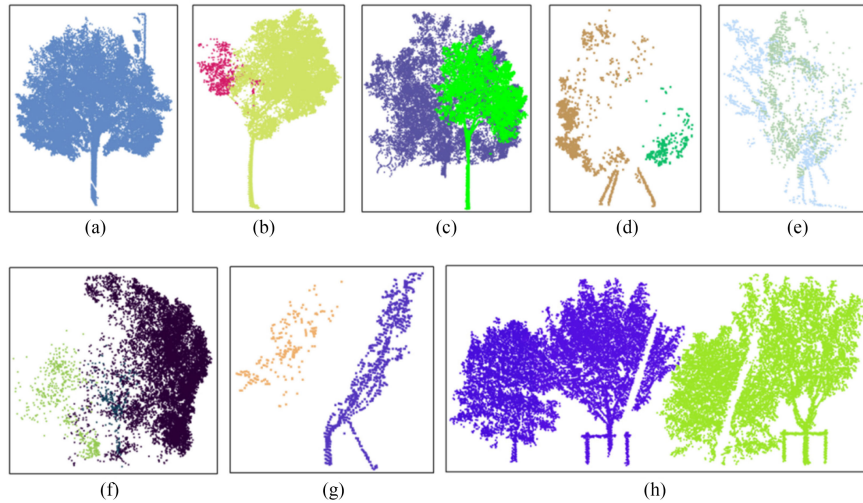


Fig. 13. Close view of the false positive results in the extraction.

TABLE IV
COMPARISON WITH OTHER INDIVIDUAL STREET TREES EXTRACTION METHODS PROPOSED FOR MLS DATA

Algorithm	Wu2013_1	Wu2013_2	Wu2016	Li2016_1	Li2016_2	Zhong2017
<i>r</i> (%)	100	100	89.0	98.5	96.3	93.7
Evaluation <i>p</i> (%)	100	98.5	86.2	100	92.9	94.0
<i>f</i>	1.00	0.99	0.88	0.99	0.95	0.94
Algorithm	Huang2015	Yadav2018	Xu2018	Improved Wu2013	Proposed	
<i>r</i> (%)	97.3	93.8	98.9	98.4	96.4	
Evaluation <i>p</i> (%)	90.8	88.2	94.0	73.8	100	
<i>f</i>	0.94	0.91	0.96	0.84	0.98	

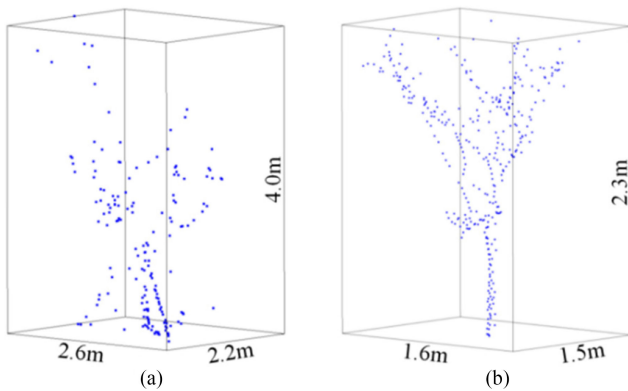


Fig. 14. Close view of the false-negative results in the extraction.

cannot be selected. This leads to serious omission of extraction. In contrast, the proposed method does not rely on the selection of seed points and can extract street trees with trunks blocked.

Table IV shows the quantitative analysis results of street trees extraction from several MLS point cloud data. It can be seen that the completeness of our method is the highest, which is 100%. Although the completeness of Wu2013_1 and Li2016_1 are also 100%, but their experimental scenes are far less complex than ours. In their test scenes, there is no crown touching of street trees, and there are no blocked trunks. In our test data, for the

street trees whose trunks are not scanned due to the block, the proposed method can still identify them correctly, and there is no missing extraction. This is not achieved by most of the existing methods based on the selection of tree trunks. For example, the completeness of the street trees extraction of the Improved Wu2013 method in our test data is only 73.8%. In terms of the correctness of street trees extraction, the correctness of our method is 96.4% which is slightly lower than that of Wu2013, Li2016_1, Huang2015, Xu2018, and Improved Wu2013. There are mainly two reasons that affect the correctness of our method. One is that in region 4 of our test data, there are two rows of street trees, and the crowns are severely blocked, which leads to incomplete crowns of some trees or too large difference in point density of the same crown [Fig. 13(b) and (f)]. Therefore, one crown is wrongly divided into two during the extraction. However, for the experimental data used in the comparison methods, there is no case of multiple rows of street trees. The other reason is that our method cannot remove the artificial irregular objects mixed in the crowns (mainly traffic signs and traffic lights, etc.) well, which is also a problem in most of the existing individual trees extraction methods. On the whole, although the data we used are more complex, the proposed method is still superior to the most existing methods. Especially for the comparison with the Improved Wu2013 method, it can be seen that the proposed method has great advantage in the extracting of street trees whose trunks are blocked.

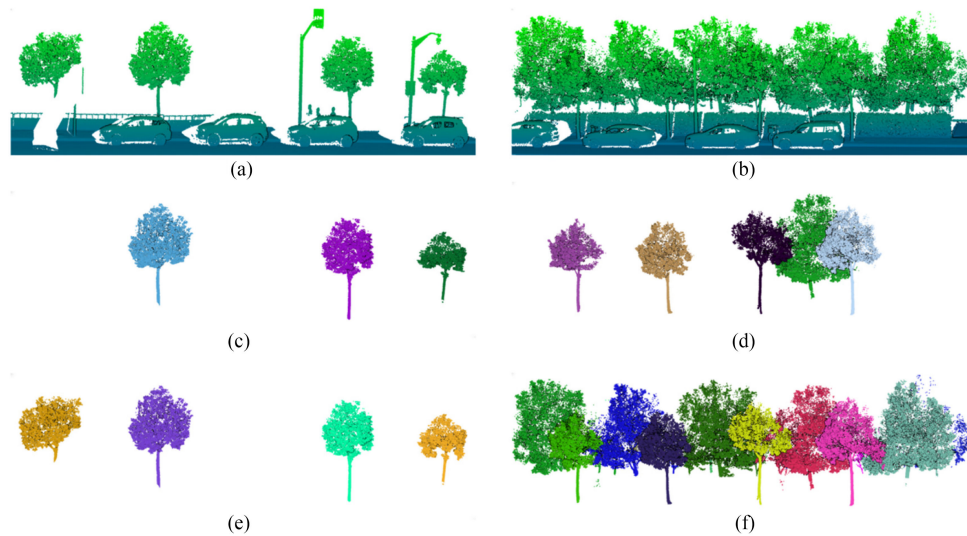


Fig. 15. Typical extraction result comparisons between two different methods. (a) and (b) are original point clouds of typical parts in region 2 and region 4, respectively; (c) and (d) are the extraction results by Improved Wu2013 method for the typical parts in region 2 and region 4, respectively; (e) and (f) are the extraction results by the proposed method for the typical parts in region 2 and region 4, respectively.

VI. CONCLUSION

For individual trees extraction from urban MLS point cloud data, we proposed an over-segmentation-based uphill clustering method, the main steps of which include the supervoxels generation, potential tree crowns and trunks determination, and individual trees extraction. Results show that it can extract individual trees in different complex scenes successfully. For the tree with blocked or missing trunk, it can still be extracted individually, which means that the proposed method does not rely on the data quality of the tree trunks.

Using the experimental data, the correctness and completeness of the proposed method for the extraction of street trees are 96.4% and 100%, respectively. There is no missing extraction and the overall extraction result is better than most existing methods. In addition, the proposed method also has a good extraction for greening trees that are heavily blocked in the green belt areas. The correctness and completeness are 83.3% and 94.6%, respectively. The content that needs further research is that the proposed individual trees extraction method has to be further improved for the extraction of street trees mixed with artificial irregular objects in the crowns.

REFERENCES

- [1] C.-F. Fang and D.-L. Ling, "Investigation of the noise reduction provided by tree belts," *Landscape Urban Plann.*, vol. 63, no. 4, pp. 187–195, May 2003.
- [2] J. Liu, Z. Xiao, Y. Chen, P. Huang, R. Wu, and J. Li, "Automated extraction of urban roadside trees from mobile laser scanning point clouds based on a voxel growing method," in *Proc. IEEE Int. Geosci. Remote Sens. Symp.*, Jul. 2017, pp. 1832–1835.
- [3] Y. Wang, H. Weinacker, and B. Koch, "A LiDAR point cloud based procedure for vertical canopy structure analysis and 3D single tree modelling in forest," *Sensors*, vol. 8, no. 6, pp. 3938–3951, Jun. 2008.
- [4] S. Xu, X. Sun, J. Yun, and H. Wang, "A new clustering-based framework to the stem estimation and growth fitting of street trees from mobile laser scanning data," *IEEE J. Sel. Topics Appl. Earth Observ. Remote Sens.*, vol. 13, pp. 3240–3250, Jun. 2020, doi: [10.1109/JSTARS.2020.3001978](https://doi.org/10.1109/JSTARS.2020.3001978).
- [5] M. Yadav and B. Lohani, "Identification of trees and their trunks from mobile laser scanning data of roadway scenes," *Int. J. Remote Sens.*, vol. 41, no. 4, pp. 1–26, Sep. 2019.
- [6] J. Wang, R. Lindenbergh, and M. Menenti, "SigVox—A 3D feature matching algorithm for automatic street object recognition in mobile laser scanning point clouds," *ISPRS J. Photogramm.*, vol. 128, pp. 111–129, Jun. 2017.
- [7] M. Soilán, A. Sánchez-Rodríguez, P. del Río-Barral, C. Perez-Collazo, P. Arias, and B. Riveiro, "Review of laser scanning technologies and their applications for road and railway infrastructure monitoring," *Infrastructures*, vol. 4, no. 4, Sep. 2019, Art. no. 58.
- [8] L. Ma, Y. Li, J. Li, C. Wang, R. Wang, and M. A. Chapman, "Mobile laser scanned point-clouds for road object detection and extraction: A review," *Remote Sens.-Basel*, vol. 10, no. 10, Sep. 2018, Art. no. 1531.
- [9] M. Yadav, A. Husain, A. K. Singh, and B. Lohani, "Pole-shaped object detection using mobile LiDAR data in rural road environments," *ISPRS Ann. Photogramm. Remote Sens. Spatial Inf. Sci.*, vol. II-3/W5, pp. 11–16, Aug. 2015.
- [10] L. Li, Y. Li, and D. Li, "A method based on an adaptive radius cylinder model for detecting pole-like objects in mobile laser scanning data," *Remote Sens. Lett.*, vol. 7, no. 3, pp. 249–258, Dec. 2015.
- [11] C. Ordóñez, C. Cabo, and E. Sanz-Ablanedo, "Automatic detection and classification of pole-like objects for urban cartography using mobile laser scanning data," *Sensors*, vol. 17, no. 7, Jun. 2017, Art. no. 1465.
- [12] F. Li, S. O. Elberink, and G. Vosselman, "Pole-like road furniture detection and decomposition in mobile laser scanning data based on spatial relations," *Remote Sens.-Basel*, vol. 10, no. 4, Mar. 2018, Art. no. 531.
- [13] N. H. Arachchige, S. N. Perera, and H.-G. Maas, "Automatic processing of mobile laser scanner point clouds for building façade detection," in *Proc. Int. Arch. Photogramm. Remote Sens. Spatial Inf. Sci.*, Jul. 2012, pp. 187–192.
- [14] Y. Li, Q. Hu, M. Wu, J. Liu, and X. Wu, "Extraction and simplification of building façade pieces from mobile laser scanner point clouds for 3D street view services," *ISPRS Int. Geo-Inf.*, vol. 5, no. 12, Dec. 2016, Art. no. 231.
- [15] L. Fang, B. Yang, C. Chen, and H. Fu, "Extraction 3D road boundaries from mobile laser scanning point clouds," in *Proc. 2nd IEEE Int. Conf. Spatial Data Mining Geographical Knowl. Serv.*, Jul. 2015, pp. 162–165.
- [16] P. Kumar, P. Lewis, and T. McCarthy, "The potential of active contour models in extracting road edges from mobile laser scanning data," *Infrastructures*, vol. 2, no. 3, p. 9, Jul. 2017.
- [17] S. Xu, R. Wang, and H. Zheng, "Road curb extraction from mobile LiDAR point clouds," *IEEE Trans. Geosci. Remote Sens.*, vol. 55, no. 2, pp. 996–1009, Feb. 2017.
- [18] C. Cabo, A. Kukko, S. García-Cortés, H. Kaartinen, J. Hyypä, and C. Ordóñez, "An algorithm for automatic road asphalt edge delineation from mobile laser scanner data using the line clouds concept," *Remote Sens.-Basel*, vol. 8, no. 9, Sep. 2016, Art. no. 740.

- [19] M. Yadav, A. K. Singh, and B. Lohani, "Extraction of road surface from mobile LiDAR data of complex road environment," *Int. J. Remote Sens.*, vol. 38, no. 16, pp. 4645–4672, May 2017.
- [20] M. Weinmann, B. Jutzi, and C. Mallet, "Semantic 3D scene interpretation: A framework combining optimal neighborhood size selection with relevant features," *ISPRS Ann. Photogramm. Remote Sens. Spatial Inf. Sci.*, vol. II–3, pp. 181–188, Sep. 2014.
- [21] B. Xiang, J. Yao, X. Lu, L. Li, and R. Xie, "Segmentation-based classification for 3D urban point clouds," in *Proc. IEEE Int. Conf. Inf. Automat.*, Aug. 2016, pp. 172–177.
- [22] L. Landrieu and M. Simonovsky, "Large-scale point cloud semantic segmentation with superpoint graphs," in *Proc. IEEE CVF Conf. Comput. Vis. Pattern Recognit.*, Jun. 2018, pp. 4558–4567.
- [23] Q. Hu, B. Yang, L. Xie, S. Rosa, and A. Markham, "RandLA-Net: Efficient semantic segmentation of large-scale point clouds," in *Proc. IEEE/CVF Conf. Comput. Vis. Pattern Recognit.*, Jun. 2020, pp. 11109–11117.
- [24] B. Yang, Y. Liu, F. Liang, and Z. Dong, "Using sing mobile laser scanning data for features extraction of high accuracy driving maps," in *Proc. Int. Arch. Photogramm. Remote Sens. Spatial Inf. Sci.*, Jun. 2016, pp. 433–439.
- [25] L. Ma, Y. Li, J. Li, Z. Zhong, and M. A. Chapman, "Generation of horizontally curved driving lines in HD maps using mobile laser scanning point clouds," *IEEE J. Sel. Topics Appl. Earth Observ.*, vol. 12, no. 5, pp. 1572–1586, May 2019.
- [26] C. Wen, X. Sun, J. Li, C. Wang, Y. Guo, and A. Habib, "A deep learning framework for road marking extraction, classification and completion from mobile laser scanning point clouds," *ISPRS J. Photogramm.*, vol. 147, pp. 178–192, Jan. 2019.
- [27] Y. Chen *et al.*, "Rapid urban roadside tree inventory using a mobile laser scanning system," *IEEE J. Sel. Topics Appl. Earth Observ. Remote Sens.*, vol. 12, no. 9, pp. 3690–3700, Sep. 2019.
- [28] G. Yue, R. Liu, H. Zhang, and M. Zhou, "A method for extracting street trees from mobile LiDAR point clouds," *Open Cybern. Syst. J.*, vol. 9, no. 1, pp. 204–209, Apr. 2015.
- [29] R. Zhong, J. Wei, W. Su, and Y. F. Chen, "A method for extracting trees from vehicle-borne laser scanning data," *Math. Comput. Model.*, vol. 58, no. 3–4, pp. 733–742, Aug. 2013.
- [30] M. Yadav, P. Khan, A. K. Singh, and B. Lohani, "Generating GIS database of street trees using mobile LiDAR data," *ISPRS Ann. Photogramm. Remote Sens. Spatial Inf. Sci.*, vol. IV–5, pp. 233–237, Nov. 2018.
- [31] B. Wu *et al.*, "A voxel-based method for automated identification and morphological parameters estimation of individual street trees from mobile laser scanning data," *Remote Sens.-Basel*, vol. 5, no. 2, pp. 584–611, Jan. 2013.
- [32] A.-V. Vo, L. Truong-Hong, D. F. Laefer, and M. Bertolotto, "Octree-based region growing for point cloud segmentation," *ISPRS J. Photogramm.*, vol. 104, pp. 88–100, Jun. 2015.
- [33] L. Li, D. Li, H. Zhu, and Y. Li, "A dual growing method for the automatic extraction of individual trees from mobile laser scanning data," *ISPRS J. Photogramm.*, vol. 120, pp. 37–52, Oct. 2016.
- [34] F. W., C. W., and J. L., "Automated extraction of urban trees from mobile LiDAR point clouds," in *Proc. 2nd ISPRS Int. Conf. Comput. Vis. Remote Sens.*, Mar. 2016, Art. no. 99010P.
- [35] L. Zhong, L. Cheng, H. Xu, Y. Wu, Y. Chen, and M. Li, "Segmentation of individual trees from TLS and MLS data," *IEEE J. Sel. Topics Appl. Earth Observ. Remote Sens.*, vol. 10, no. 2, pp. 774–787, Feb. 2017.
- [36] H. Guan, Y. Yu, Z. Ji, J. Li, and Q. Zhang, "Deep learning-based tree classification using mobile LiDAR data," *Remote Sens. Lett.*, vol. 6, no. 11, pp. 864–873, Sep. 2015.
- [37] P. Huang, Y. Chen, J. Li, Y. Yu, C. Wang, and H. Nie, "Extraction of street trees from mobile laser scanning point clouds based on subdivided dimensional features," in *Proc. IEEE Int. Geosci. Remote Sens. Symp.*, Jul. 2015, pp. 557–560.
- [38] M. Weinmann, M. Weinmann, C. Mallet, and M. Brédif, "A classification-segmentation framework for the detection of individual trees in dense MMS point cloud data acquired in urban areas," *Remote Sens.-Basel*, vol. 9, no. 3, Mar. 2017, Art. no. 277.
- [39] S. Xu, N. Ye, S. Xu, and F. Zhu, "A supervoxel approach to the segmentation of individual trees from LiDAR point clouds," *Remote Sens. Lett.*, vol. 9, no. 6, pp. 515–523, Feb. 2018.
- [40] S. Xu, S. Xu, N. Ye, and F. Zhu, "Automatic extraction of street trees' non-photosynthetic components from MLS data," *Int. J. Appl. Earth Observ.*, vol. 69, pp. 64–77, Jul. 2018.
- [41] S. Xia, D. Chen, R. Wang, J. Li, and X. Zhang, "Geometric primitives in LiDAR point clouds: A review," *IEEE J. Sel. Topics Appl. Earth Observ. Remote Sens.*, vol. 13, pp. 685–707, Feb. 2020, doi: [10.1109/JS-TARS.2020.2969119](https://doi.org/10.1109/JS-TARS.2020.2969119).
- [42] Y. Yu, J. Li, H. Guan, C. Wang, and J. Yu, "Semiautomated extraction of street light poles from mobile LiDAR point-clouds," *IEEE Trans. Geosci. Remote Sens.*, vol. 53, no. 3, pp. 1374–1386, Mar. 2015.
- [43] Y. Lin, C. Wang, D. Zhai, W. Li, and J. Li, "Toward better boundary preserved supervoxel segmentation for 3D point clouds," *ISPRS J. Photogramm.*, vol. 143, pp. 39–47, Sep. 2018.
- [44] J. Papon, A. Abramov, M. Schoeler, and F. Worgotter, "Voxel cloud connectivity segmentation-supervoxels for point clouds," in *Proc. IEEE Conf. Comput. Vis. Pattern Recognit.*, Jun. 2013, pp. 2027–2034.
- [45] D. Zai *et al.*, "3-D road boundary extraction from mobile laser scanning data via supervoxels and graph cuts," *IEEE Trans. Intell. Transp. Syst.*, vol. 19, no. 3, pp. 802–813, Mar. 2018.
- [46] Q. Li and X. Cheng, "Comparison of different feature sets for TLS point cloud classification," *Sensors*, vol. 18, no. 12, Nov. 2018, Art. no. 4206.
- [47] Y. Li, B. Wu, and X. Ge, "Structural segmentation and classification of mobile laser scanning point clouds with large variations in point density," *ISPRS J. Photogramm.*, vol. 153, pp. 151–165, Jun. 2019.
- [48] R. B. Rusu and S. Cousins, "3D is here: Point cloud library (PCL)," in *Proc. IEEE Int. Conf. Robot. Automat.*, May 2011, pp. 1–4.
- [49] H. Hoppe, T. DeRose, T. Duchamp, J. McDonald, and W. Stuetzle, "Surface reconstruction from unorganized points," *ACM SIGGRAPH Comput. Graph.*, vol. 26, no. 2, pp. 71–78, Jul. 1992.
- [50] B. Yang, Z. Dong, G. Zhao, and W. Dai, "Hierarchical extraction of urban objects from mobile laser scanning data," *ISPRS J. Photogramm.*, vol. 99, pp. 45–57, Jan. 2015.



Jintao Li received the B.S. degree in surveying and geoinformatics from Shandong University of Science and Technology, Qingdao, China, in 2018. He is currently working toward the Ph.D. degree with the Surveying and Mapping Science and Technology at the College of Surveying and Geo-Informatics, Tongji University, Shanghai, China.

His research interests include LiDAR data processing and mobile mapping.



Xiaojun Cheng received the B.S., M.S., and Ph.D. degrees in surveying and geoinformatics from Tongji University, Shanghai, China, in 1985, 1992, and 2002, respectively.

He is currently a Full Professor with the College of Surveying and Geo-Informatics, Tongji University. His research interests include digital close-range photogrammetry and 3-D digital simulation.



Zhenlun Wu received the B.S. degree in traffic and transportation engineering from Changsha University of Science & Technology, Changsha, China, in 2016, and the M.S. degree in surveying and mapping science and technology from Tongji University, Shanghai, China, in 2019.

He joined the Big Data Development Administration of Yichun after graduation and has been working on a variety of solutions to smart city and 3-D reconstruction of city projects both inside and outside China. His research interests include LiDAR data processing, multisource data fusion, and BIM Technology.



Wang Guo received the B.S. degree in GIS from Zhengzhou University, Zhengzhou, China, in 2006, the M.S. degree in hyper-information system from Zhengzhou University, Zhengzhou, China, in 2013, and the Ph.D. degree in surveying and geoinformatics from Tongji University, Shanghai, China, in 2018.

He is currently the Product Director in mobile mapping business segment with CHC Navigation Ltd., Company His research interests include LiDAR data acquisition, LiDAR data processing, and multisource data fusion.